

# Shade Resilient PV Panel Architecture

Filipe Oliveira

filipe.a.g.oliveira@tecnico.ulisboa.pt

September 2021

## Abstract

This work aims to develop and study an architecture of photovoltaic panels, power converters and Maximum Power Point Tracking (MPPT) system capable of solving the partial shading problem.

Firstly, the evolution of the installed photovoltaic capacity and the costs of photovoltaic modules in the world is presented, followed by an explanation of the shading problem.

The model used to characterize photovoltaic modules and panels is presented, allowing its study using simulations in a MATLAB/Simulink environment. The most common methods of MPPT are reviewed, highlighting their main characteristics. The proposed architecture of photovoltaic panels to solve the shading problem is presented, as well as the Ćuk converter used, making an analysis of its operation and presenting the sizing of its elements. A new type of MPPT system is developed and a non-linear current controller is implemented for the input current of the series connected Ćuk converters. A single-phase grid-tie inverter is also designed, with linear and non-linear controllers for the inverter's direct voltage and alternating current being developed.

The results obtained with the proposed architecture are compared with those obtained using the standard architecture with a series connection of photovoltaic modules and a single converter responsible for the MPPT. The simulation results show that the proposed architecture can solve the shading problem, extracting more power than that of the standard architecture, and very close to the theoretical power predicted for a shaded photovoltaic panel.

**Keywords:** Shading, PV panels; MATLAB/Simulink Simulation, Ćuk

## 1. Introduction

Possible consequences of the so-called climate change can pose one of the biggest threats to different areas of society these days. Greenhouse gases such as  $\text{CO}_2$ , produced in part by burning fossil fuels to meet our energy needs, are generally seen as causing widespread warming, so it is urgent to invest in clean and sustainable energy production. One of the most promising renewable energy sources is photovoltaic solar energy, which has shown significant growth in installed capacity around the world [1].

Solar energy can be transformed into electrical energy using photovoltaic cells that use the photovoltaic effect to generate an electrical current when subjected to sunlight [2].

The most common photovoltaic cells on the market are crystalline silicon cells, due to their reduced cost, stability, reliability, abundance of silicon and high efficiency – 24.4% in laboratory environment for the best performing monocrystalline modules [3].

Between 2010 and 2020, the average efficiency of photovoltaic modules on the market increased from 12% to 17% [4]. Furthermore, be-

tween 2011 and 2017, the average production cost of photovoltaic modules built with crystalline silicon technologies dropped from US\$1.59/Wp to US\$0.34/Wp [5].

Due to the reduced voltage and power obtained from a single photovoltaic cell, several cells are connected in series, forming photovoltaic modules [6]. To obtain higher power, the photovoltaic modules can be aggregated forming what can be called a photovoltaic panel [6].

Generally, a single power converter is used to perform the Maximum Power Point Tracking (MPPT) of the panel, placing bypass diodes at the terminals of each module, as shown in Figure 1.

Under uniform irradiance, the PV panel's P-V curve has a unique Maximum Power Point. However, when under non-uniform irradiance, the PV panel's P-V curve has multiple local maxima, as shown in Figure 2, where three PV modules were connected in series with irradiances of  $500\text{W}/\text{m}^2$ ,  $300\text{W}/\text{m}^2$  and  $200\text{W}/\text{m}^2$ .

This behaviour is due to the bypass diodes that are usually installed in photovoltaic modules in order to avoid the appearance of hot spots [7]. In Figure 2, the Maximum Power Point reaches 232, 8W.

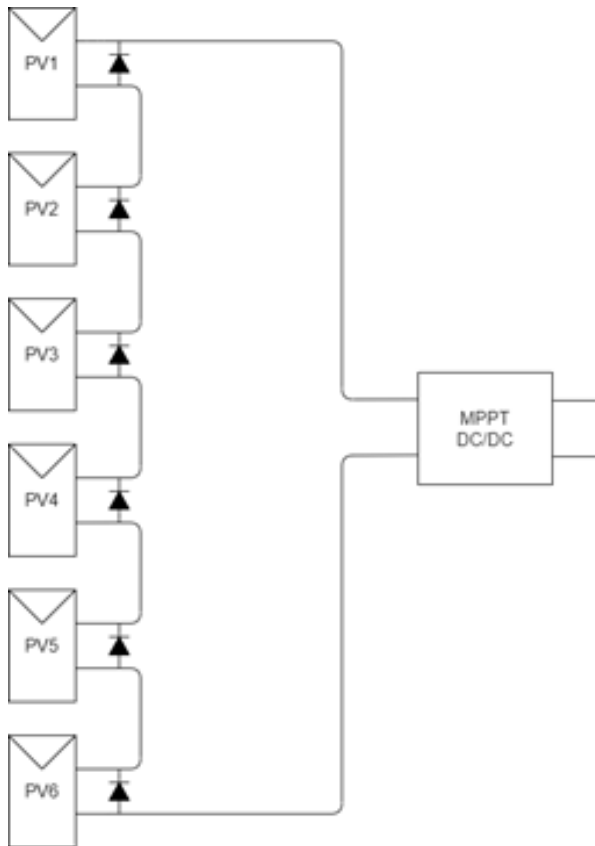


Figure 1: Common PV Panel Architecture with 6 PV Modules

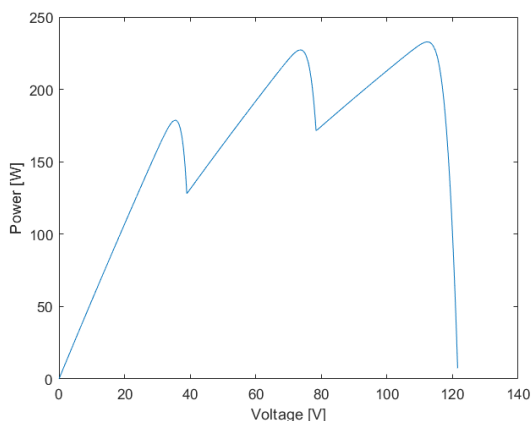


Figure 2: P-V Curve for shaded panel consisting of 3 PV Modules in series

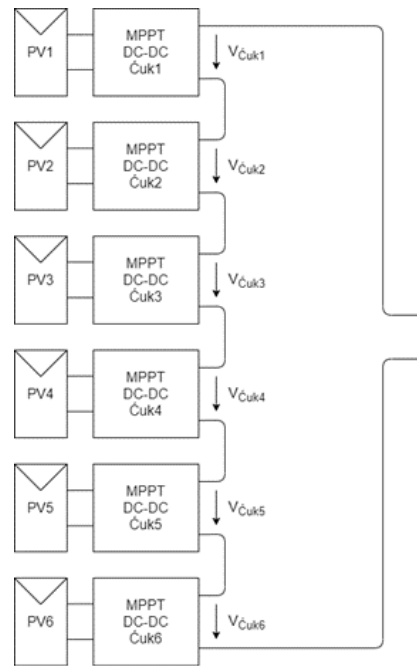


Figure 3: Proposed PV Panel Architecture with 6 PV Modules

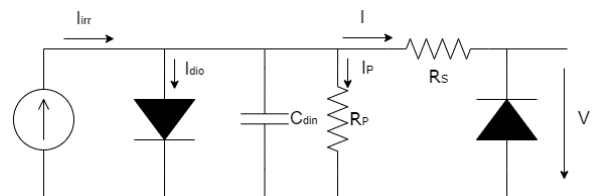


Figure 4: One diode and five parameters equivalent circuit

However, if each PV module operated in its individual Maximum Power Point, the sum of the output power of the modules would be 357,7W - significantly higher than the power obtained with the common PV architecture.

In order to solve the above-described shading problem, a shade resilient PV panel architecture is proposed - Figure 3 - where each PV module is connected to a  $\hat{C}uk$  Converter responsible for MPPT.

## 2. PV Model

In order to study the behavior of the PV modules and panels under different irradiance and temperature conditions in a simulation software such as MATLAB/Simulink, a mathematical model is needed. The mathematical model used to describe each PV module is based on the "one diode and five parameters" model presented in [8], shown in Figure 4.

The specifications provided by the module's manufacturer are presented in Table 1 and the obtained parameters for the equivalent circuit, according to [8] are shown in Table 2.

To account for the dynamic behaviour of the module/panel,  $C_{din} = 3,5\mu F$

**Table 1:** Module specifications provided by the Manufacturer

Maximum Power [W]	Pmax	375
MPP Voltage [V]	Vmpp	37,2
MPP Current [A]	Impp	10,09
Open Circuit Voltage [V]	$V_{OC}$	42,8
Short Circuit Current	$I_{SC}$	10,83
Nominal Operating Cell Temperature [°C]	NOCT	44
$V_{OC}$ Temperature Coefficient [%/°C]	$\beta'_T$	-0,24
$I_{SC}$ Temperature Coefficient [%/°C]	$\alpha'_T$	0,037

**Table 2:** Equivalent Circuit model parameters

$I_{irr,ref}$ [A]	10,94
$I_{0,ref}$ [pA]	2,31
$n_{ref}$	0,95
$R_{P,ref}$ [ $\Omega$ ]	75,45
$R_{S,ref}$ [ $\Omega$ ]	0,076

### 3. Ćuk Converter, MPPT & Control

#### 3.1. Ćuk Converter

With the objective of obtaining high efficiency in the power converter connected to each PV module, the Ćuk Converter was chosen for this implementation, since it has the advantage that its input current is not pulsed. A capacitor is added to the converter's input, as shown in Figure 5.

According to [9],  $L_1$  and  $C_1$  are sized similarly to the Boost Converter and  $L_2$  and  $C_2$  are sized similarly to the Buck Converter:

$$L_1 = \frac{V_{PV} T}{4\Delta i_{L1}} = \frac{V_o (1-\delta)^2}{\frac{\Delta i_{L1}}{I_{L1}} I_{L2}} \quad (1)$$

$$C_1 = \frac{I_{L1} \delta T}{\Delta V_{C1}} = \frac{I_{L2} \frac{\delta^3}{1-\delta} T}{\frac{\Delta V_{C1}}{V_o}} \quad (2)$$

$$L_2 = \frac{V_{PV} \delta T}{\Delta i_{L2}} = \frac{V_o (1-\delta) T}{\Delta i_{L2}} \quad (3)$$

$$C_2 = \frac{T \Delta i_{L2}}{8 \Delta V_o} \quad (4)$$

where

$\delta$  - Duty cycle

$\Delta$  - Maximum ripple

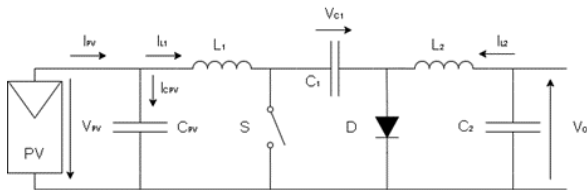


**Figure 5:** Proposed Ćuk Converter

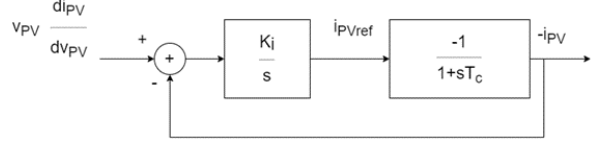


**Figure 6:** MPPT controller model block diagram

The sizing of  $C_{PV}$  is derived from its charge variation:

$$C_{PV} = \frac{T \Delta i_{L1}}{8 \Delta V_{PV}} \quad (5)$$

#### 3.2. MPPT

An Incremental Conductance (IncCond) based MPPT system was developed, due to its good performance under rapidly changing irradiance conditions [10]. The control objective is

$$\frac{dP_{PV}}{dv_{PV}} = 0 \quad (6)$$

Knowing that at the Maximum Power Point  $\frac{dP_{PV}}{dv_{PV}} = 0$  and that the power output of the PV module is given by  $P_{PV} = v_{PV} i_{PV}$ , at the Maximum Power Point one can write

$$\frac{dP_{PV}}{dv_{PV}} = v_{PV} \frac{di_{PV}}{dv_{PV}} + i_{PV} \quad (7)$$

Equation (7) represents the ideal MPPT behavior. However, in practice, it is impossible to guarantee a null error at all times. Therefore, it can be assumed that  $v_{PV} \frac{di_{PV}}{dv_{PV}}$  has some error or deviation  $e_{MPP}$  that has to be enforced to approach zero in a finite time interval.

$$v_{PV} \frac{di_{PV}}{dv_{PV}} + i_{PV} = e_{MPP} \quad (8)$$

A linear controller can be devised to enforce the error  $e_{MPP}$  to converge to zero, noting that:

$$v_{PV} \frac{di_{PV}}{dv_{PV}} - (-i_{PV}) = e_{MPP} \quad (9)$$

Therefore,  $-i_{PV}$  must follow the value  $v_{PV} \frac{di_{PV}}{dv_{PV}}$ . Suppose the converter, when driven by a current controller with input  $i_{PVref}$ , returns the value  $-i_{PV}$  with a dynamics of a low pass filter with pole at  $-\frac{1}{sT_C}$ :

$$-i_{PV} = -i_{PVref} \frac{1}{1 + sT_C} \quad (10)$$

A linear integral controller  $\frac{K_i}{s}$  can then be devised to ensure MPPT tracking (with zero steady-state error) as shown in Figure 6.

From Figure 6, the closed-loop transfer function is

$$\frac{-i_{PV}}{v_{PV} \frac{di_{PV}}{dv_{PV}}} = \frac{-\frac{K_i}{T_C}}{s^2 + \frac{s}{T_C} - \frac{K_i}{T_C}} \quad (11)$$

Comparing the closed-loop to the canonical form of a second-order system  $s^2 + 2\xi_A\omega_n s + \omega_n^2$

$$\begin{cases} \omega_n^2 = \frac{-K_i}{T_C} \\ K_i = -\frac{1}{4\xi_A^2 T_C} \end{cases} \quad (12)$$

The time constant  $T_C$  can be estimated considering the  $C_{PV}$  capacitor at the output of the PV panel loaded by an equivalent resistor given by  $R_{PV} = \frac{v_{op}}{i_{op}}$ , where  $v_{op}$  and  $i_{op}$  are the maximum power point voltage and current of the PV module or panel, being  $T_C = C_{PV}R_{PV}$ .

### 3.3. Input Current Control

To maintain the PV module operating at its maximum power point, it is necessary to design a current controller that opens/closes the switch S of the Ćuk Converter, following  $i_{PVref}$ .

For the Ćuk Converter in Figure 5, according to [11]:

$$\frac{di_{L1}}{dt} = \frac{V_{PV} - \gamma_C V_{C1}}{L_1} \quad (13)$$

where

$$\gamma_C = \begin{cases} 1 & \rightarrow \text{S OFF \& D ON} \\ 0 & \rightarrow \text{S ON \& D OFF} \end{cases} \quad (14)$$

Since  $V_{C1} > V_{PV}$ , the dynamics of  $i_{L1}$  depends only on  $\gamma_C$ .

$$\gamma_C = \begin{cases} 1 & \Rightarrow \frac{di_{L1}}{dt} < 0 \\ 0 & \Rightarrow \frac{di_{L1}}{dt} > 0 \end{cases} \quad (15)$$

Ideally,  $i_{L1}$  should follow  $i_{PVref}$  with zero error  $e_{iL1}$ .

$$e_{iL1} = i_{PVref} - i_{L1} = 0 \quad (16)$$

However, the converter is switched at finite frequency, making it impossible for the instantaneous error to be null at all times. The current  $i_{L1}$  has a ripple component that can be considered as an error. This error can be forced to approach zero, varying the  $i_{L1}$  and, in turn, the error in the range  $-\varepsilon < e_{iL1} < \varepsilon$ . Therefore, a hysteresis comparator with width  $2\varepsilon$  allows to define  $\gamma_C$ :

$$e_{iL1} > \varepsilon \Rightarrow i_{PVref} > i_{L1} \Rightarrow i_{L1} \uparrow \Rightarrow \frac{di_{L1}}{dt} > 0 \Rightarrow$$

$$\Rightarrow \gamma_C = 0 \quad (17)$$

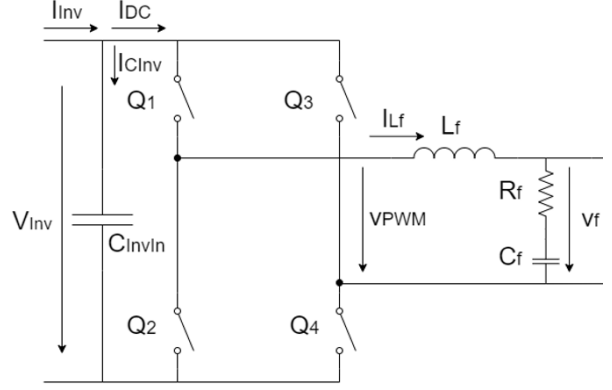


Figure 7: Single-Phase Inverter

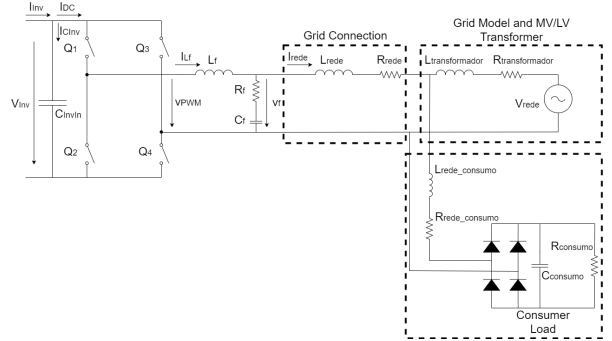


Figure 8: Grid Connection and Grid Model

$$\begin{aligned} e_{iL1} < -\varepsilon \Rightarrow i_{PVref} > i_{L1} \Rightarrow i_{L1} \downarrow \Rightarrow \frac{di_{L1}}{dt} < 0 \Rightarrow \\ \Rightarrow \gamma_C = 1 \end{aligned} \quad (18)$$

## 4. Grid-Tie Inverter

Taking into account the proposed architecture (Figure 3) with six PV modules with peak power  $P_P = 375W_P$ , a single-phase Grid-Tie inverter was used - Figure 7.

The connection to the grid is done through a cable and the grid is modelled as a transformer feeding a rectifier with an R||C load, as shown in Figure 8.

### 4.1. Filter Sizing

For the sizing of the inverter's components, the grid is considered as a load resistor:

$$R_{eq} = \frac{V_{rede}}{I_{rede}} = \frac{V_{rede}^2}{P_{AC}} \quad (19)$$

where  $P_{AC}$  is the power delivered to the grid.

For a given damping factor  $\xi_B$ , the characteristic impedance of the filter can be estimated

$$Z_{char} = 2\xi_B R_{eq} \quad (20)$$

From the grid frequency  $\omega_{rede}$  and the switching frequency  $\omega_{comutacao}$ , the cutoff frequency of the

filter  $\omega_{res}$  can be estimated

$$\omega_{res} \approx \sqrt{\omega_{rede}\omega_{comutacao}}$$

Filter elements  $C_f$  and  $L_f$  are then given by

$$C_f = \frac{1}{\omega_{res}Z_{char}} \quad (21)$$

$$L_f = \frac{Z_{char}}{\omega_{res}} \quad (22)$$

With the purpose of damping oscillations,  $R_f$  is added in series to  $C_f$ . Choosing a value for the damping coefficient  $\xi_C$ ,  $R_f$  is given by

$$R_f = 2\xi_C \frac{1}{\omega_{res}C_f} \quad (23)$$

The input capacitor is obtained through

$$C_{InvIn} = \frac{I_{Inv}}{\Delta v_{Inv}\omega_{rede}} \quad (24)$$

## 4.2. Control

### 4.2.1 Linear Control

For the linear control, a carrier-based modulator is used. For the AC current control, the converter and modulator are represented by a first-order function with gain  $K_D$  and delay  $T_{di}$  [12].

$$G_{MC}(s) = \frac{K_D}{1 + sT_{di}} \quad (25)$$

$K_D$  is given by

$$K_D = \frac{V_{Inv}}{u_{Cmax}} \quad (26)$$

A linear proportional-integral controller can then be devised, ensuring zero steady-state error:

$$C(s) = \frac{1 + sT_z}{sT_p} \quad (27)$$

Considering that the pole with the lowest frequency introduced by the filter is cancelled by the zero of the compensator,  $T_z$  is calculated by

$$T_z = \frac{L_f}{R_{eq}} \quad (28)$$

$T_p$  is given by

$$T_p = \frac{2K_D T_{di}}{R_{rede}} \quad (29)$$

The reference current value is obtained by making the control objective a constant voltage across  $C_{InvIn}$  - Voltage  $V_{Inv}$ . The dynamics of  $V_{Inv}$  can be described through

$$V_{Inv} = \frac{1}{sC_{InvIn}}(I_{Inv} - I_{DC}) \quad (30)$$

The current control loop can then be represented by  $\frac{G}{1+sT_d}$  where  $G = \frac{V_{redeRMS}}{V_{Inv}}$ . A linear proportional-integral controller is then devised:

$$C_{1PV}(s) = \frac{1 + sT_{zv}}{sT_{pv}} \quad (31)$$

The controller gains are then calculated through

$$\begin{cases} \omega_0 = \frac{1}{1,75T_d} \\ T_{pv} = \frac{-1,75^3 T_d^2 G}{C_{InvIn}} \\ T_{zv} = 2,15 \times 1,75 \times T_d \end{cases} \quad (32)$$

The value obtained through this controller is the peak value of the sinusoidal current to be injected into the grid. Therefore, this value has to be multiplied by a unity amplitude sinusoid and synchronized with the mains voltage. This synchronism is done using a PLL.

### 4.2.2 Non-Linear Control

Non-linear current control is based on the dynamics of  $i_{L_f}$

$$\frac{di_{L_f}}{dt} = \frac{v_{PWM} - v_f}{L_f} \quad (33)$$

with

$$v_{PWM} = \gamma_D V_{Inv}$$

where

$$\gamma_D = \begin{cases} 1 \rightarrow Q_1 \wedge Q_4 ON \\ 0 \rightarrow Q_1 \wedge Q_3 \vee Q_2 \wedge Q_4 ON \\ -1 \rightarrow Q_2 \wedge Q_3 ON \end{cases}$$

This means that the dynamics of  $i_{L_f}$  depend on  $\gamma_D$ .

The controller aims to ensure that the converter follows a current reference. The error is

$$e_{i_{L_f}} = i_{L_f,ref} - i_{L_f} \quad (34)$$

In order to force  $e_{i_{L_f}}$  to tend to zero, it is necessary to guarantee  $\frac{de_{i_{L_f}}}{dt} < 0$ . For this to happen depending on the sign of  $e_{i_{L_f}}$ , the sign of the derivative is determined through  $\gamma_D$ , assuming  $V_{Inv} > V_f$

$$\begin{cases} di_{L_f} > 0, \gamma_D = 1 \\ i_{L_f} < 0, \gamma_D = -1 \\ e_{i_{L_f}} \approx 0, \gamma_D = 0 \end{cases}$$

The current  $i_{L_f}$  has ripple  $\Delta i_{L_f}$  and a maximum acceptable value can be defined for this same ripple by choosing  $\gamma_D$  based on the error value. The

range  $\frac{-\Delta i_{L_f}}{5} < e_{i_{L_f}} < \frac{\Delta i_{L_f}}{5}$  was chosen so that the system can operate with  $\gamma_D = 0$ , allowing the inverter to operate with three levels of output voltage decreasing harmonic distortion.

The reference current value is obtained by making the control objective a constant voltage across  $C_{InvIn}$  - Voltage  $V_{Inv}$ . The dynamics of  $V_{Inv}$  can be described through

$$C_{InvIn} \frac{dV_{Inv}}{dt} = (i_{Inv} - i_{DC}) \quad (35)$$

Multiplying the two members of the equation by  $V_{Inv}$ :

$$V_{Inv} C_{InvIn} \frac{dV_{Inv}}{dt} = V_{Inv} i_{Inv} - V_{Inv} i_{DC} \quad (36)$$

Considering that  $V_{Inv} i_{DC}$  is the input power of the inverter:

$$V_{Inv} i_{DC} = \frac{V_{f_{RMS}} I_{L_f RMS} f_p}{\eta} \quad (37)$$

where  $f_p$  is the power factor and  $\eta$  the efficiency. Substituting (37) in (36)

$$\frac{C_{InvIn}}{2} \frac{dV_{Inv}^2}{dt} = V_{Inv} i_{Inv} - \frac{V_{f_{RMS}} I_{L_f RMS} f_p}{\eta} \quad (38)$$

The current is injected into the grid synchronized with the voltage, guaranteeing  $f_p \approx 1$ . Therefore, the quantity  $V_{Inv}^2$  can then be controlled by controlling the current  $I_{L_f RMS}$ .

The control of the current  $I_{L_f RMS}$  can be done using Lyapunov's direct method [13]

We then define an error function and a positive definite Lyapunov function:

$$e_{V_{Inv}^2} = V_{ref}^2 - V_{Inv}^2 \quad (39)$$

$$L_\lambda = \frac{e_{V_{Inv}^2}}{2} \quad (40)$$

From Lyapunov's direct method

$$\frac{de_{V_{Inv}^2}}{dt} + Ke_{V_{Inv}^2} = 0, K > 0 \quad (41)$$

Substituting (39) in (41) and considering  $V_{ref}^2$  constant

$$-\frac{dV_{Inv}^2}{dt} = -Ke_{V_{Inv}^2} \quad (42)$$

Through mathematical manipulation of (38)

$$I_{L_f RMS} = \frac{\eta C_{InvIn}}{2V_{ref} f_p} \left( -Ke_{V_{Inv}^2} + \frac{2}{C_{InvIn}} V_{Inv} i_{Inv} - \frac{dV_{Inv}^2}{dt} \right) \quad (43)$$

**Table 3:** Cuk Converter Filter Elements

$C_{PV} [\mu F]$	40,45
$C_1 [\mu F]$	33,5
$C_2 [\mu F]$	4,22
$L_1 [mH]$	4,3
$L_2 [mH]$	1,8

where  $\frac{dV_{Inv}^2}{dt} \approx 0$  and  $f_p \approx 1$ .

The value obtained through this controller is the RMS value of the sinusoidal current to be injected into the grid. Therefore, this value has to be multiplied by a sinusoid with amplitude  $\sqrt{2}$  and synchronized with the mains voltage. This synchronism is done using a PLL.

## 5. Results & Discussion

In order to obtain comparative results, two systems were designed:

- Proposed Architecture
- Common Architecture - Series connection of PV modules

### 5.1. Sizing

#### 5.1.1 Proposed Architecture

In order to proceed with the sizing of the filter elements, it is necessary to establish an operating interval for the duty cycle. For this, extreme operating conditions of the photovoltaic modules are considered:

- Irradiance  $G = 100W/m^2$  and Ambient Temperature  $T_{amb} = -25^\circ C$ . Under these conditions  $V_{PV} = 40, 27V$
- Irradiance  $G = 1000W/m^2$  and Ambient Temperature  $T_{amb} = 50^\circ C$ . Under these conditions  $V_{PV} = 31, 18V$

Choosing  $V_{Inv} = 400V$ , with uniform irradiance on the PV panel, the output voltage of each Cuk Converter is  $V_o = 66,67V$ . From here, the operation range for the duty cycle is obtained  $\delta \in [0, 62; 0, 68]$ .

Maximizing the filter values, choosing ripples  $\Delta i_{L1} = 2,5\%$ ,  $\Delta i_{L2} = 10\%$ ,  $\Delta V_{PV} = 0,1\%$ ,  $\Delta V_o = 0,1\%$ ,  $\Delta V_{C1} = 10\%$  and assuming a switching frequency  $f = 1/T = 25kHz$  the values present in Table 3 are obtained.

The connection between the panel and the inverter is considered to have an inductance of  $50\mu H$ .

The MPPT system gain  $K_i$  is calculated by choosing  $\xi_A = 3$  and considering the MPP voltage and current:

$$K_i = -186,26$$

For the desired ripple for the input current of  $2,5\%$ , the hysteresis comparator operates with window  $[-0,13; 0,13]A$ .

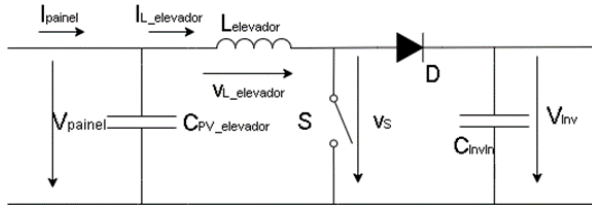


Figure 9: Boost Converter for MPPT

Table 4: Boost Converter Filter Elements

$C_{PV\_elevador} [\mu F]$	6,74
$L_{elevador} [mH]$	20,4

### 5.1.2 Series Connection of PV Modules

For this architecture, a Boost converter is used to perform the MPPT (Figure 9).

The Boost Converter is connected to the Inverter's input capacitor.

The Capacitor  $C_{PV\_elevador}$  is sized similarly to  $C_{PV}$ ;

$$C_{PV\_elevador} = \frac{T \Delta i_{L\_elevador}}{8 \Delta V_{paineil}} \quad (44)$$

The inductor  $L_{elevador}$  is given by

$$L_{elevador} = \frac{V_{paineil} \delta T}{\Delta i_{L\_elevador}} \quad (45)$$

To proceed with the sizing of the filter elements, it is necessary to establish an operating interval for the duty cycle and for  $V_{paineil}$ .

Considering the previously presented range of voltages for a single PV module, the PV panel range of voltages is  $V_{paineil} \in [187, 1; 241, 6]V$ .

By choosing, once again,  $V_{Inv} = 400V$ , the operation range for the duty cycle is obtained  $\delta \in [0, 40; 0, 53]$ .

Maximizing the filter values, choosing ripples  $\Delta i_{L\_elevador} = 2,5\%$ ,  $\Delta V_{paineil} = 0,1\%$  and assuming a switching frequency  $f = 1/T = 25kHz$  the values present in Table 4 are obtained.

The connection between the panel and the Boost Converter is considered to have an inductance of  $50\mu H$ .

The MPPT system gain  $K_i$  is calculated by choosing  $\xi_A = 3$  and considering the MPP voltage and current ( $V_{op} = 223, 20V$  and  $I_{op} = 10, 09A$ ):

$$K_i = -186, 26$$

For the desired ripple for the input current of 2,5%, the hysteresis comparator operates with window  $[-0, 13; 0, 13]A$ .

### 5.1.3 Inverter

Choosing  $V_{Inv} = 400V$  and a maximum ripple  $\Delta V_{Inv} = 5\%$

$$C_{InvIn} = 895, 25\mu F$$

Considering for the grid nominal voltage  $V_{rede} = 230V$  and maximum power  $P_{AC} = 2250W$  and  $\xi_B = \frac{\sqrt{2}}{2}$

$$Z_{char} = 33, 2\Omega$$

Considering a switching frequency  $f_{comutacao}$  of 5 kHz and grid frequency 50 Hz:

$$C_f = 9, 7\mu F$$

$$L_f = 10, 7mH$$

Choosing  $\xi_C = 0, 5$ , to ensure reduced power loss in  $R_f$

$$R_f = 33, 2\Omega$$

### Linear Control

Considering the grid frequency of 50 Hz, the delay is  $T_d = \frac{1}{2 \times 50}$  and  $G = \frac{230}{400}$ . From here, the controller parameters are:

$$T_{zv} = 0, 0376$$

$$T_{pv} = -0, 3442$$

The current control parameters are dependant on the switching frequency of the inverter and will be designed once the switching frequency of the non-linear controller is known, allowing for a fair comparison of the two control systems.

### Non-Linear Control

The designed controller features first-order dynamics, with  $1/K$  time constant.  $K$  must be defined in such a way that the response time of the system is not smaller than the period of the mains voltage, taking the value  $K_{max} = 50$  as a limit for  $K$ . To maintain reduced current waveform distortion and a fast response of the system,  $K=10$  was chosen.

### 5.2. Grid Model

The interter is connected to the electrical grid through a cable with impedance:

$$R_{rede} = 0, 19\Omega$$

$$L_{rede} = 0, 03mH$$

A grid transformer of 750kVA with  $R=0,004$  pu and  $L=0,16$  pu is used

$$R_{transformador} = 853, 34\mu\Omega$$

$$L_{transformador} = 108, 65\mu H$$

To include the harmonic distortion caused by grid consumers, a rectifier with a  $R||C$  load is connected to the transformer

$$R_{consumo} = 10\Omega$$

$$C_{consumo} = 5mF$$

### 5.3. Simulation Results

To obtain comparative results between the two architectures presented, two possible irradiance scenarios are considered. Let  $G_{1-6}$  be the incident irradiances on modules PV1 to PV6.

- Scenario A:  $G_{1-6} = 1000\text{W/m}^2$
- Scenario B:  $G_1 = 300\text{W/m}^2$ ,  $G_{2-3} = 500\text{W/m}^2$  and  $G_{4-6} = 1000\text{W/m}^2$

The behavior of the two architectures is analyzed in a sequence that goes from scenario A to scenario B and again to scenario A, in a simulation lasting 3,5s, with transitions occurring at 1,5s and 2,5s.

An ambient temperature of  $20^\circ\text{C}$  is considered.

#### Series Connection of PV Modules

The inverter control system does not change the power output of the PV panel significantly. The power output for the Series Connection of PV Modules is shown in Figure 10.

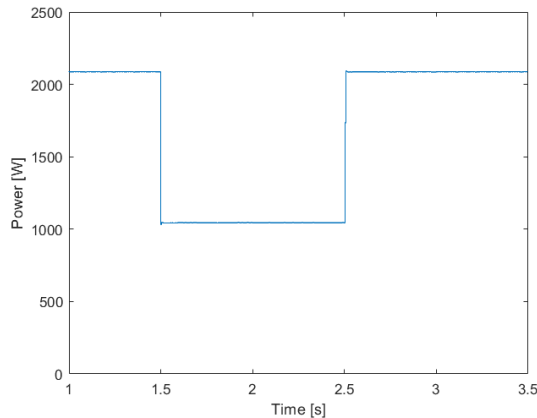


Figure 10: Power Output of the PV Panel

In scenario A, the PV Panel outputs 2087,6 W (close to the theoretical value 2092,2 W) and in scenario B the PV panel outputs 1044,3 W.

#### Series Connection of PV Modules - Non-Linear Inverter Control

The voltage  $V_{Inv}$  is shown in Figure 11.

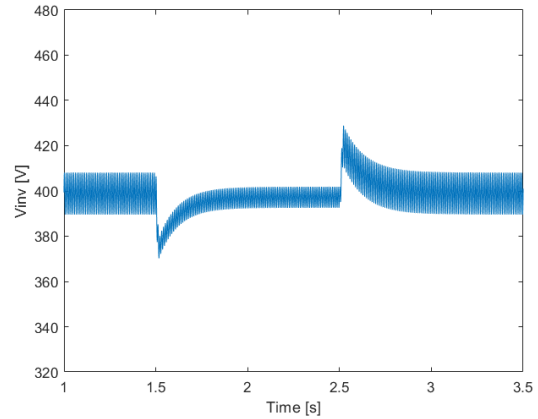


Figure 11: Voltage across the inverter's input Capacitor

The harmonic content of  $V_f$  is shown in Figure 12.

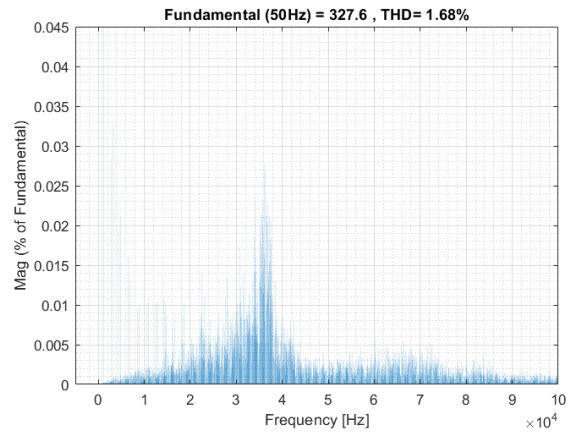


Figure 12: Harmonics of  $V_f$

#### Series Connection of PV Modules - Linear Inverter Control

As seen in Figure 12, the inverter's switching frequency is around 35kHz. The current control parameters are

$$T_z = 7,9511 \times 10^{-5}$$

$$T_p = 4,6849 \times 10^{-4}$$

The voltage  $V_{Inv}$  is shown in Figure 13.



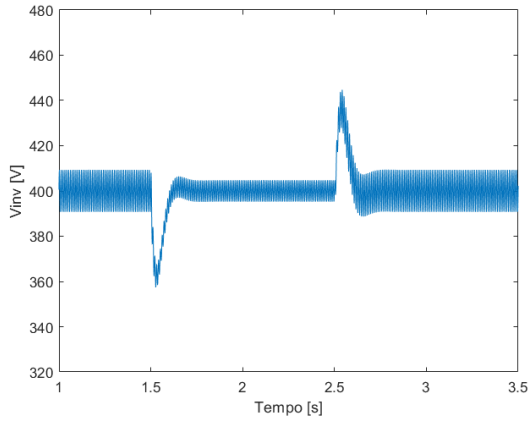


Figure 13: Voltage across the inverter's input Capacitor

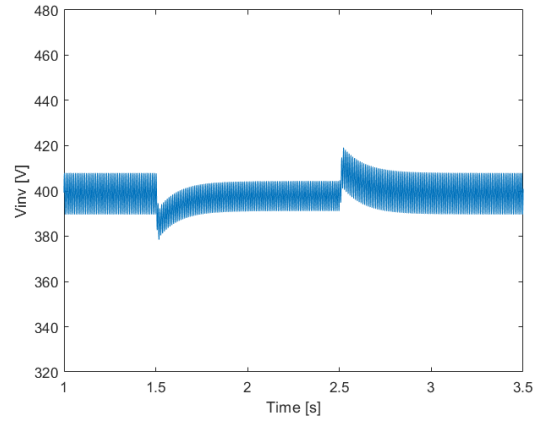


Figure 15: Voltage across the inverter's input Capacitor

### Proposed Architecture

The inverter control system does not change the power output of the PV panel significantly. The power output for the Proposed Architecture is shown in Figure 14.

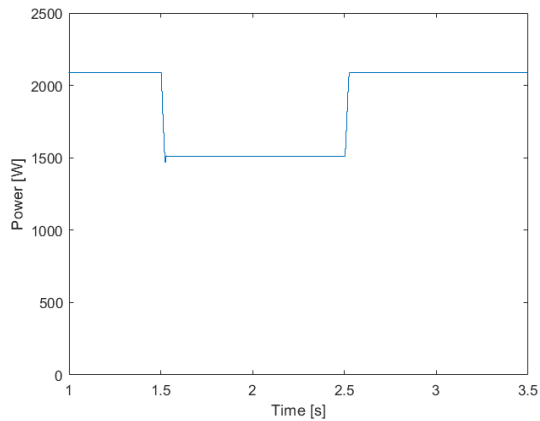


Figure 14: Power Output of the PV Panel

In scenario A, the PV Panel outputs 2089,6 W (close to the theoretical value 2092,2 W) and in scenario B the PV panel outputs 1509,3 W.

### Proposed Architecture - Non-Linear Inverter Control

The voltage  $V_{Inv}$  is shown in Figure 15.

### Proposed Architecture - Linear Inverter Control

For an inverter switching frequency of 35kHz. The current control parameters are

$$T_z = 7,9511 \times 10^{-5}$$

$$T_p = 4,6849 \times 10^{-4}$$

The voltage  $V_{Inv}$  is shown in Figure 16.

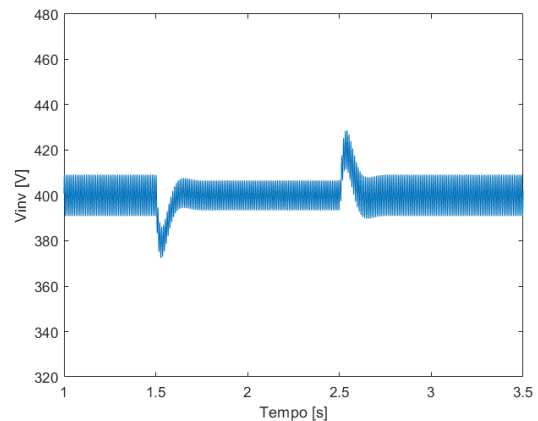


Figure 16: Voltage across the inverter's input Capacitor

Tables 5 and 6 summarize the obtained results with both architectures

### 6. Conclusions

When the panel is subjected to uniform irradiance conditions, it is observed that the two architectures presented approach the maximum power point. However, the greatest discrepancy occurs for non-uniform irradiance conditions. In scenario B, the maximum power point of the series connection of PV modules reaches 1045,9 W, around 2/3 of the maximum power that is possible to reach with the proposed architecture – 1511,3 W. The implemented system reached 1044.3 W with the series connection of photovoltaic modules against

1509,3 W with the proposed architecture. The proposed architecture allows each of the modules to remain at its maximum power point, regardless of the conditions to which the other modules are subject, which does not happen in the series connection of PV modules, in which the modules subject to lower irradiances are short circuited by the bypass diodes and there is no guarantee that the other modules will operate at their maximum power point.

**Table 5:** Obtained Results with the Series Connection of PV Modules

		Series Connection of PV Modules	
		Linear Inverter Control	Non-Linear Inverter Control
Power	Scenario A	2087,6 W	2087,6 W
	Scenario B	1044,3 W	1044,3 W
THDv	Scenario A	1,66%	1,68%
	Scenario B	1,68%	1,69%
THDi	Scenario A	3,97%	2,08%
	Scenario B	4,14%	2,04%

**Table 6:** Obtained Results with the Proposed Architecture

		Proposed Architecture	
		Linear Inverter Control	Non-Linear Inverter Control
Power	Scenario A	2089,3 W	2089,3 W
	Scenario B	1509,3 W	1509,3 W
THDv	Scenario A	1,66%	1,67%
	Scenario B	1,67%	1,68%
THDi	Scenario A	3,91%	2,05%
	Scenario B	3,95%	1,90%

In the studied cases, the inverter control method does not affect the power delivered to it. Voltage THD is similar for the two implemented control methods. However, the non-linear inverter control has an advantageous behavior, namely a significantly lower current THD - for similar powers obtained with the two architectures presented (irradiance scenario A), the non-linear inverter control obtains a current THD of 2.08% for the standard architecture and 2.05% for the proposed architecture against 3,97% and 3.91% for linear control of the inverter. The non-linear control of the inverter has a faster response to sudden changes in power supplied to the inverter, which translate into smaller changes in voltage at the inverter input capacitor terminals.

## References

- [1] SolarPower Europe (2020): Global Market Outlook for Solar Power 2020-2024
- [2] M. V. Anne Labouret, "Solar Photovoltaic Energy," The Institution of Engineering and Technology, 2010.
- [3] M. K. S. D. J. P. J. K. S. K. M. J. Y. K. Y. C., C. C. J. Y. Sanchari Chowdhury, "High-efficiency Crystalline Silicon Solar Cells: A Review," *New & Renewable Energy*, vol. 15, n<sup>o</sup> 3, pp. 36-45, 2019.
- [4] F. f. S. EnergySystems, "Photovoltaics Report," 2019.
- [5] Fischer, "ITRPV 9th edition 2018 report release and key findings," 2018.
- [6] R. Castro, "Uma Introdução Às Energias Renováveis: Eólica, Fotovoltaica e Mini-Hídrica," IST Press, Lisboa, 2018.
- [7] G. M. L. V. L. M. R. F. R. F. Anotnino Laudani, "On circuital topologies and reconfiguration strategies for PV systems in partial shading conditions: a review," *AIMS Energy*, vol. 6, 2017.
- [8] F. M.-D. K. E. P. J. Hongmei Tian, "A Detailed Performance Model for Photovoltaic Systems," *Solar Energy Journal*, 2012.
- [9] J. Kassakian, M. Schlecht, & G. Verghese, *Principles of Power Electronics*, MA, EUA: Addison-Wesley, 1991.
- [10] H. B. F. K. Boualem Bendib, "A survey of the most used MPPT methods: Conventional and advanced algorithms applied for photovoltaic systems," *Renewable and Sustainable Energy Reviews*, vol. 45, pp. 637-648, 2015.
- [11] J. F. A. Silva, *Electrónica Industrial*, Lisboa: Fundação Calouste Gulbenkian, 2013.
- [12] S. P. J. S. Fernando Silva, *Conversores Comutados para Energias Renováveis*, Lisboa, 2016.
- [13] Martin, A. D., Cano, J. M., Silva, J. F. A., & Vazquez, J. R. (2015). Backstepping control of smart grid-connected distributed photovoltaic power supplies for telecom equipment. *IEEE Transactions on Energy Conversion*, 30(4), 1496–1504.